Chapter 10 Undersea Amplified Lightwave Systems Design

Neal S. Bergano

AT&T Laboratories, Holmdel, New Jersey

10.1 Introduction

The erbium-doped fiber amplifier (EDFA) has had a profound impact on the design, operation, and performance of transoceanic cable transmission systems and is central to the expected proliferation of undersea cable networks. The first long-haul amplifier systems were installed in 1995 with a single 5-Gb/s optical channel, twice the capacity of the most advanced digital regenerator-based fiber system in use. Laboratory experiments have demonstrated in excess of 100 Gb/s over transoceanic distances using wavelength-division multiplexing (WDM) techniques. This large transmission capacity will make possible the deployment of new systems concepts such as optical undersea networks. Systems based on the new optical amplifier technology promise to satisfy the international transmission needs into the 21st century.

Undersea cable systems have a long history of providing international connectivity of terrestrial communications networks. The first successful transoceanic cable system was deployed in 1866 in the North Atlantic and provided telegraph service from North America to Europe (Thiennot, Pirtio, and Thomine 1993). It took about 90 years from the time of the first successful telegraph cable until the first transatlantic telephone cable was installed. The first transatlantic telephone cable was commissioned in 1956 and provided 48 voice channels using coaxial cable and repeaters with vacuum tube amplifiers (Ehrbar 1986). Since the first telephone cable systems were installed, the capacity of transatlantic cable's circuits

OPTICAL FIBER TELECOMMUNICATIONS, VOLUME IIIA

ISBN: 0-12-395170-4

has increased at an annual rate of 20–27% (Fig. 10.1). New innovations, rather than a single technology, have allowed capacity to keep pace with demand. Coaxial systems technology progressed through the 1960s and 1970s to include better cables and transistor amplifiers, eventually providing 10,000 voice circuits in systems deployed in the late 1970s and early 1980s.

The first fiber optic systems were installed in the Atlantic and Pacific oceans in 1988 to 1989 and operated at 280 Mb/s per fiber pair. These were actually hybrid optical systems in the sense that the repeaters converted the incoming signals from optical to electrical, regenerated the data with high-speed integrated circuits, and retransmitted the data with a local semiconductor laser. The transmission capacity of the regenerated fiber cables eventually increased to 2.5 Gb/s, and repeater spacing increased with the switch from 1.3-μm multifrequency lasers to 1.55-μm single-frequency laser diodes. The first fiber systems greatly improved the quality of international telephony; however, the ability of the regenerator systems to exploit the large fiber bandwidth were limited by the capacity bottleneck in the high-speed electronics of undersea

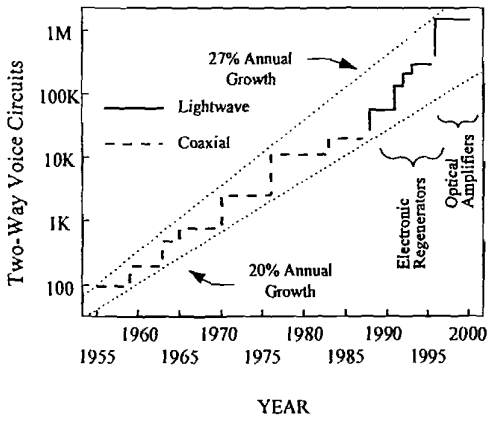

Fig. 10.1 This figure shows the cumulative number of *voice* circuits installed across the Atlantic by AT&T and its partners during the past four decades. For the coaxial cables, a circuit multiplication factor of two is assumed for each 3-kHz channel using Time Assignment Speech Interpolation (TASI). For the digital cables, a circuit multiplication factor of five is assumed for each 64-kB/s channel using digital speech compression.

repeaters. Undersea lightwave systems with EDFA repeaters remove the electronic bottleneck and provide the first clear optical channel connectivity between the world's continents.

This chapter reviews important concepts for the design of long-haul transmission systems based on optical amplifier repeaters and the non-return-to-zero (NRZ) modulation format. When possible, the reader is directed to other chapters of this book for an expanded explanation of concepts, such as amplifier design. The first sections give a comparison of the different modulation formats considered useful to long-haul communications systems. The next few sections lead the reader through a description of amplifier chains, dispersion management, measures of system performance, important polarization effects, and long-haul transmission measurements. Finally, a description of a typical long-haul optical amplifier system is given.

10.2 Transmission Formats

Although lightwave systems are known to be at the cutting edge of technology, the basic signaling format for most systems is simple. Most lightwave systems use direct detection of amplitude shift keyed light pulses to send binary information. Binary ones and zeros are sent by the presence or the absence of light pulses, much as one could imagine using a flashlight with an on–off switch to convey a string of ones and zeros. A transmission system based on this simple pulse scheme is referred to as a *unipolar pulse system* (Bell Telephone Laboratories 1982). Most often, the light pulse that is used is a rectangular pulse that occupies the entire bit period, which is referred to as an *NRZ format* (Fig. 10.2). The term *NRZ* attempts to describe the waveform's constant value characteristic when consecutive binary ones are sent (Fig. 10.3). Alternatively, a string of binary data with optical pulses that do not occupy the entire bit period are described generically as *RZ,* or *return-to-zero.* Two common examples of RZ signaling pulses are the rectangular pulse that occupies one-half of the bit period, and a hyperbolic secant squared pulse (or soliton) with a pulse width of about one-fifth the time slot.

The two interesting signaling formats for use in long-haul transmission systems are NRZ and solitons (see Chapter 12 in Volume IIIA for a complete description of solitons). Table 10.1 lists some of the strengths and weaknesses of both formats. Most long-haul lightwave systems in use today

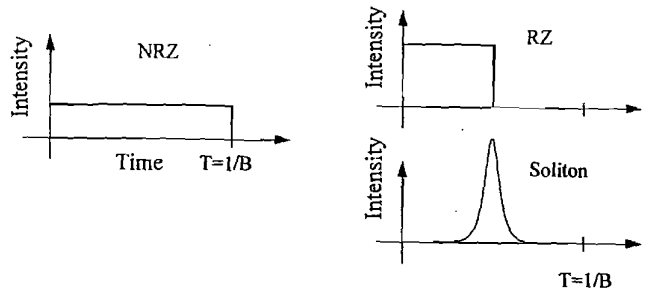

Fig. 10.2 Different unipolar binary code signaling pulses. NRZ, non-return to zero; RZ, return to zero.

use the NRZ signaling format because it is easy to generate, detect, and process. The NRZ transmitter is simpler to construct than the soliton transmitter. Actually, the electronics for the two are similar; however, the soliton transmitter requires an optical pulse source. The quality of the optical pulse source depends on the soliton control technique being used in the transmission line. Soliton systems will probably require some form of jitter control (Mecozzi *et al.* 1991; Kodama and Hasegawa 1992; Mollenauer, Gordon, and Evangelides 1992), which complicates the design of the amplifier chain. Line monitoring (Chapter 2 in Volume IIIB) is an issue for soliton systems, whereas it is well understood for NRZ. The single-channel

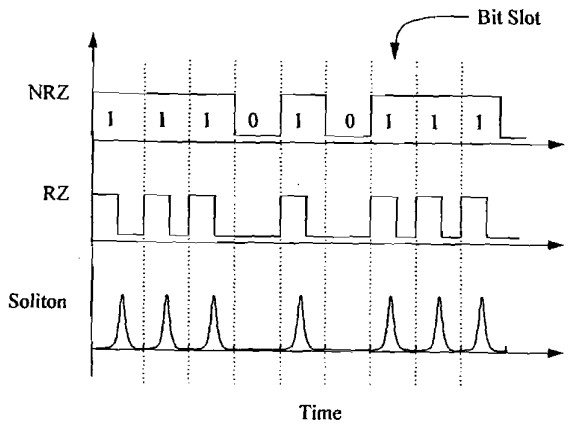

Fig. 10.3 Data waveforms for three pulse formats.

Table 10.1 **Comparison between the NRZ and Soliton Transmission Formats**

NRZ Format	*Soliton Format*
Simpler transmitter	More complex transmitter
Simpler amplifier chain	More complex amplifier chain
More tolerant to power fluctuations	Less tolerant to power fluctuations
Line monitoring understood	Line monitoring an issue
Single-channel capacity of ~10 Gb/s	Single-channel capacity of ~20 Gb/s
WDM $\Delta\lambda > 0.5$ nm	WDM $\Delta\lambda > 0.3$ nm
Amplifier gain spectrum more important for WDM systems	Amplifier gain spectrum less important for WDM systems
Wavelength stability less important	Wavelength stability more important
Synergy with existing systems	

capacity of soliton systems is probably larger than that of NRZ systems; however, large-capacity growth will come through WDM techniques. The question of which transmission format will be more useful for future systems is still open and depends on the system's requirements. For example, a system that needs to achieve the maximum total transmission capacity while utilizing the full EDFA optical bandwidth might benefit from the NRZ format. Alternatively, a system having fewer channels with the maximum bit rate per channel might make better use of the soliton format. Ultimately, the transmission format of choice will be the one that can best use the available EDFA bandwidth in a simple and reliable design.

It is interesting to ask "What ever happened to coherent communications for long-haul systems?" The introduction of the EDFA into the long-haul market greatly reduced research and development of coherent communications because many of the potential benefits of using such communications could be achieved more economically by using EDFAs. For example, very high receiver sensitivity is easily achieved using standard transmission equipment with a simple EDFA preamplified receiver. Also, coherent transmission does not work well with optically amplified lines. In optical amplifier systems, optical phase is not well maintained because of the nonlinear mixing of signal and noise (Gordon and Mollenauer 1990). Thus, direct detection of amplitude shift keying has been the clear winner in long-haul systems to date.

10.3 Amplifier Chains

The EDFA is a nearly ideal building block for providing optical gain in a lightwave communications system (Li 1993). EDFAs can be made with a variety of gains in the low-loss 1550-nm wavelength window of telecommunications fibers, with nearly ideal noise performance (see Chapter 2 Volume IIIB). EDFAs amplify high-speed signals without distortion or cross talk between wavelengths, even when the amplifier is operated deep in gain compression (Giles, Desurvire, and Simpson 1989). Because the EDFA is a fiber device, it can be easily connected to telecommunications fiber with low loss and low polarization dependence. Most important, EDFAs can be manufactured with the 25-year reliability that is required for use in undersea systems.

The undersea portion of the transmission system is essentially a chain of concatenated amplifiers and cable sections. The EDFA provides optical gain to overcome attenuation in the lightwave cable, similar to the way that electrical amplifiers were used to overcome attenuation in coaxial cable in the older style of analog undersea cables. The design of the amplifier chain must provide control of the optical power level, must address control of noise accumulation, must provide an adequate optical bandwidth for the data channels, and must minimize pulse distortion caused by chromatic dispersion and nonlinear effects.

The optical power level launched into the transmission fiber can be controlled by the natural gain saturation of the EDFAs (Fig. 10.4). Self-

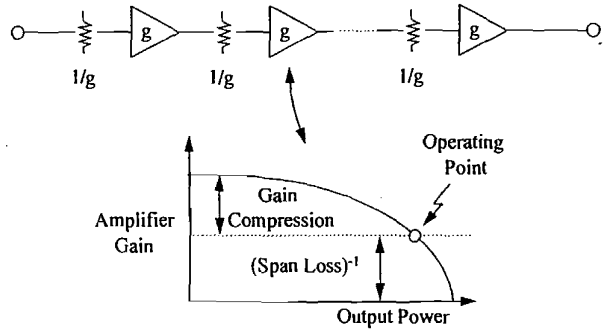

Fig. 10.4 The amplifier's output power is controlled by operating each erbium-doped fiber amplifier (EDFA) with 3–5 dB of gain compression. Steady-state operation occurs where gain equals inverse attenuation in the spans.

regulation is achieved by making the EDFA's small signal gain several decibels larger than is needed to compensate for the span's attenuation. This creates a stable operating point where amplifier gain equals span loss. If the input power to the amplifier decreases, its gain increases, and vice versa, thus the power level remains stable (Fig. 10.5).

The natural automatic gain control forces a balance of amplifier's gain and span's attenuation for signals near the system's gain peak, which occurs at the wavelength of maximum gain for the amplifier–span combination. When a 1480-nm pumped EDFA is operated with several decibels of gain compression, the gain peak occurs at the long-wavelength edge of the pass-band near 1558 nm. Figure 10.6 shows the gain and amplified spontaneous emission (ASE) noise of an EDFA operated with 5 dB of gain compression. The wavelength of the gain peak depends most strongly on the average inversion in the erbium-doped fiber (Chapter 3 in Volume IIIB), and to a lesser extent on the gain shape of the components that make up the remainder of the amplifier chain.

The usable bandwidth of a single EDFA is generally accepted to span a wavelength range of about 35 nm (1530–1565 nm). However, for a long chain of 1480-nm pumped amplifiers operated in gain compression, the usable bandwidth is substantially less. A transatlantic length system of 6300 km would require 140 amplifier spans of 45 km. The 10-dB bandwidth of a system using 140 1480-nm pumped EDFAs with 9.5-dB net gain is about 3.5 nm as shown in Figure 10.7. Unless some form of gain equalization is used, only about 10% of the EDFA's intrinsic bandwidth is available for the transmission of data. This bandwidth is large enough for a single-

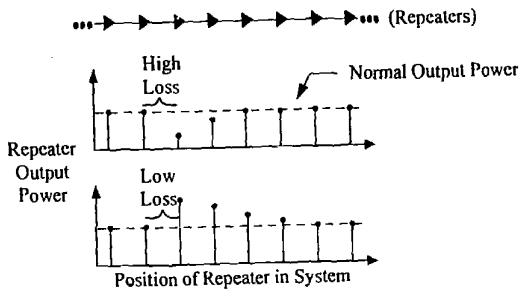

Fig. 10.5 Repeater output power versus transmission distance. The repeater's output power is controlled by gain compression in the amplifiers.

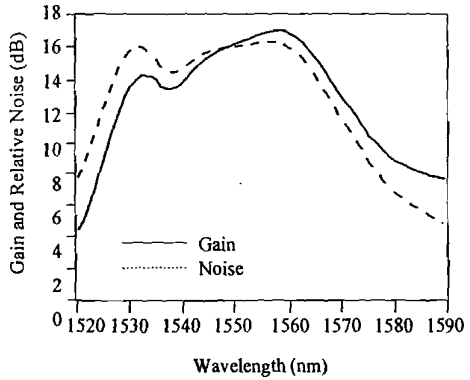

Fig. 10.6 Gain and relative output noise from a single EDFA in gain compression. Note that the gain peak occurs near 1558 nm.

channel system, but is inadequate for many WDM channels. Thus, some form of gain equalization is needed.

The usable bandwidth of a long amplifier chain can be significantly increased by using passive gain equalizing filters. The idea of gain equalization is conceptually simple; gain equalizing filters are designed to approximate the inverse characteristic of the combination of EDFA and fiber span.

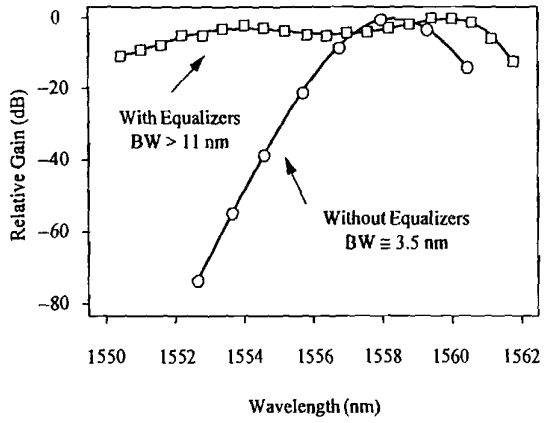

Fig. 10.7 Relative gain versus wavelength for a 6300-km amplifier chain, with and without passive gain equalization. Each symbol shows a gain measurement.

In practice, it is often more simple to design gain equalizers that correct for several amplifier spans. This has the advantage of using fewer devices, at the expense of a larger insertion loss for each equalizer. One promising technique of making gain equalizing filters uses long-period fiber grating filters (Vengsarkar *et al.* 1995), which can be made temperature insensitive (Judkins *et al.* 1996) with low back reflection, low polarization dependent loss, and low polarization mode dispersion. For example, in the WDM experiments outlined in Section 10.7, long-period fiber grating equalizers were designed to correct for the gain-shape of 8 to 10 amplifiers, with a goal of expanding the usable bandwidth by two or three times. As a practical matter, the midband loss of the filters were made similar to a typical fiber span (9.5 dB). Thus, the excess loss in the equalizing filter could be compensated using an additional amplifier of the same design as the span amplifier. Figure 10.7 shows the gain profile of the amplifier chain with and without the gain equalizers. At 6300 km, the 10-dB spectral width of the system was over 11 nm with the filters, compared to 3.5 nm without the filters. Thus, for this arrangement more than a three-fold improvement in the unstable optical bandwidth was obtained.

In a long transmission line, ASE noise generated in the EDFAs can accumulate to power levels similar to the data carrying signal. The accumulated noise can influence the system's performance by reducing the level of the signal and the signal-to-noise ratio (SNR). The noise power out of an optical amplifier is proportional to the amplifier's gain and is given by

$$P_n = 2n_{sp}h\nu(g - 1)B_o, \tag{10.1}$$

where $h\nu$ is photon energy, g is gain in linear units, n_{sp} is the excess noise factor related to the amplifier's noise figure, and B_o is optical bandwidth. As a consequence, the spectral density of the accumulated noise at the end of the system depends on the repeater gain and fiber loss. Consider the system with a fiber loss of 0.2 dB/km. A 150-km repeater spacing would require 30-dB amplifiers, whereas a 50-km spacing would need three times as many 10-dB amplifiers. A 30-dB amplifier (1000x gain) generates about 100 times more noise per unit bandwidth than that of a 10-dB gain amplifier. Thus, the 30-dB gain system would have 33 times more noise than that of the 10-dB gain system. The relationship between accumulated noise and amplifier gain imposes an interesting tradeoff; longer systems require shorter repeater spacing to keep the same output SNR.

The excess noise generated as a consequence of the amplifier's gain was described by Gordon and Mollenauer (1991). The excess noise is the factor

by which the amplifier's *output power* must increase to maintain a constant received SNR. Lichtman (1993a) embellished this description to include excess loss in the amplifiers. The excess noise is given by

$$\text{Excess noise} = \frac{g\beta - 1}{\beta \ln g}, \tag{10.2}$$

where β is postamplifier loss (Fig. 10.8). The β term is added because in a real amplifier there is always some loss that follows the erbium-doped fiber, such as an isolator or a wavelength selective coupler. The most important result of adding the postamplifier loss is that the optimum repeater spacing is not zero (pure distributed gain); rather, it occurs between 10 and 20 km.

The total accumulated noise power depends on the amount of noise generated at each amplifier (Eq. [10.1]) times the number of amplifiers in the system. As stated previously, the automatic control obtained through the amplifier's gain saturation fixes the total output power. This total power contains both signal and accumulated noise. Because the total power is fixed and noise accumulates, the signal's power must decrease as the signal propagates down the amplifier chain (Giles and Desurvire 1991). Figure 10.9 shows a measurement of signal power and accumulated noise power versus transmission distance for a single 5-Gb/s channel propagating over 10,000 km.

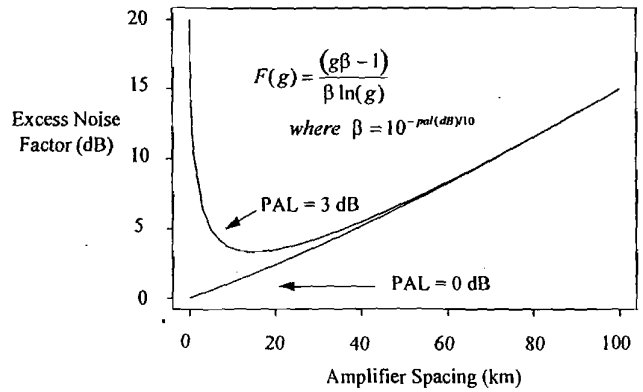

Fig. 10.8 Excess noise factor for having lumped amplifiers, assuming 0.2-dB/km fiber loss. The top curve is calculated for a postamplifier loss (PAL) of 3 dB, and the bottom curve for 0 dB.

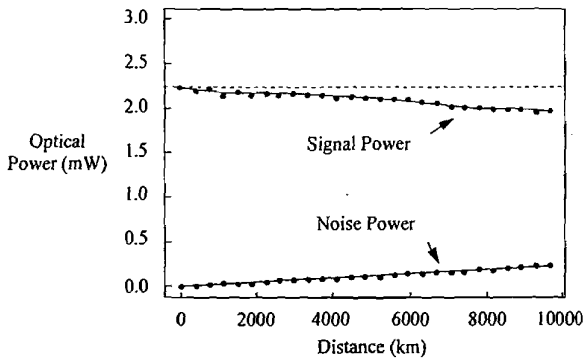

Fig. 10.9 Signal power and amplified spontaneous emission (ASE) noise power versus transmission distance for a single 5-Gb/s data signal. The *dashed horizontal line* indicates the initial launch signal power.

A simple but useful estimate of the SNR at the output of a chain of N amplifiers is

$$SNR_o = \frac{P_L}{NF(gh\nu B_o N)}, \tag{10.3}$$

where P_L is the average optical power launched into the transmission spans, NF is noise figure, g is the amplifier's gain, and B_o is optical bandwidth in hertz. Equation (10.3) assumes that all the amplifiers are identical and that there is no signal decay from noise accumulation.

10.4 Dispersion and Nonlinearity Management

Several phenomena limit the transmission performance of long-haul optical transmission systems, including noise, dispersion, and nonlinearities. For long systems, the nonlinear refractive index can couple different signal channels and can couple the signal with noise. Single-mode fibers are slightly nonlinear as a result of the dependence of the fiber's index on the intensity of the light propagating through it. This behavior is expressed as

$$n = n_0 + \frac{N_2 P}{A_{eff}}, \tag{10.4}$$

where n_0 is the linear part of the refractive index, N_2 is the nonlinear

coefficient ($\sim 2.6 \times 10^{-16}$ cm^2/W), P is the light power in the fiber, and A_{eff} is the effective area over which the power is distributed (Marcuse, Chraplyvy, and Tkach 1991). This nonlinear behavior causes only minute changes in the group velocity of the fiber. For example, the presence or absence of a 1-mW signal changes the index by 35 trillionths of a percent. The equivalent length change of 3.5 μm over the 10,000-km system is of no direct consequence to system performance; however, the time shifts are significant when one is considering optical phase. The nonlinear index leads to important phenomena such as self-phase modulation, cross-phase modulation, and four-wave mixing (Chapter 8 in Volume IIIA).

Until recently, the conventional thinking was that the maximum system bandwidth occurred for operation around the zero-dispersion wavelength in the fiber. However, this rule of thumb is not complete when one is considering fiber nonlinearities. When the system is operated at the fiber's zero-dispersion wavelength, the data signals and the amplifier noise (with wavelengths similar to the signal) travel at similar velocities. Under these conditions, the signal and noise waves have long interaction lengths and can mix. Chromatic dispersion causes different wavelengths to travel at different group velocities in single-mode transmission fiber (see, for example, Agrawal 1989a or Kaiser and Keck 1988). Chromatic dispersion can reduce phase matching, or the propagation distance over which closely spaced wavelengths overlap, and can reduce the amount of interaction through the nonlinear index in the fiber. Thus, in a long undersea system, the nonlinear behavior can be managed by tailoring the dispersion accumulation so that the phase-matching lengths are short and the end-to-end dispersion is small. This technique is known as *dispersion mapping* (see Chapter 8 in Volume IIIA). An example is shown in Fig. 10.10. This figure shows the accumulated dispersion versus transmission distance for an eight-channel WDM transmission experiment. About 900 km of single-mode dispersion-shifted fiber with a λ_0 = 1585 nm is used for every 100 km of conventional single-mode fiber with λ_0 = 1310 nm. The signal wavelengths are in the range of 1556–1560 nm. Thus, the nonlinear mixing is minimized by reducing the interaction lengths, and the distortion of the data is minimized by ensuring that the total dispersion returns to zero at the end of the system.

An important observation for WDM systems is that the accumulated dispersion returns to zero for only one wavelength near the average zero-dispersion wavelength for the transmission line. This is seen in Fig. 10.10

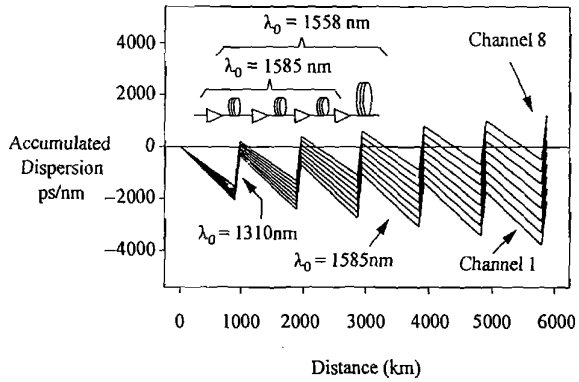

Fig. 10.10 Dispersion map showing the accumulated chromatic dispersion versus transmission distance for eight channels of a wavelength-division multiplexing (WDM) transmission experiment. Most amplifier spans use negative-dispersion fiber with $\lambda_0 = 1585$ nm and $D \cong -2$ ps/km-nm. The dispersion is compensated for every 1000 km using conventional single-mode fiber (i.e., $\lambda_0 = 1310$ nm).

by the diverging lines for channels 1 through 8. Obviously, this is of no consequence for single-channel systems where the end-to-end zero-dispersion wavelength is simply made to coincide with the operating wavelength. However, it is important for WDM systems. This differing accumulated dispersion for the WDM channels results from the nonzero slope of the dispersion curve. The linear approximation for dispersion versus wavelength (near λ_0) is

$$D(\lambda) = SL(\lambda - \lambda_0) , \qquad (10.5)$$

where D is dispersion, S is dispersion slope (~0.07 ps/km-nm^2), L is fiber length, λ_0 is zero-dispersion wavelength, and λ is wavelength. To minimize signal distortion, the accumulated dispersion for the channels away from λ_0 can be compensated for with the opposite dispersion at the receiver.

10.5 Measures of System Margin

The most important feature of a digital transmission system is the ability to operate with a small bit error rate (BER). In fact, most digital transmission systems operate with BERs that are too small to be practically measured. This is especially true at the beginning of life for an undersea system where

extra margin has been added to the design to allow for the system to age. When a system is installed, it is necessary that it performs with a low error rate, but this is not a sufficient characteristic to ensure that the system has an adequate margin against SNR fluctuations and aging. What is required is an accurate measure of system margin. System margin is defined as the difference (measured in decibels) in the received SNR and the SNR required to maintain a given BER. In long-haul lightwave systems, the BER is set by a combination of the electrical SNR of the data signal at the decision circuit, and any distortions in the data's waveform. The BER is degraded by optical noise, fiber chromatic dispersion, polarization mode dispersion, fiber nonlinearities, and changes in the receiver. Also, the BER can fluctuate with time as a result of polarization effects in the transmission fiber and the amplifier's components.

A measure of the system's performance must properly include both the random noise and the pattern-dependent effects that can degrade the BER. Accumulated noise adds random fluctuations to the received data and has the effect of closing the received eye diagram with an unbounded noise process. Noise accumulation alone does not change the underlying shape of the transmitted waveform. The primary source of the noise is the accumulated ASE from the EDFAs. Pattern dependence, or intersymbol interference (ISI), limits transmission performance by changing the shape of the received waveform. Many effects contribute to ISI, including nonideal transmitters and receivers, chromatic dispersion, polarization dispersion, and fiber nonlinearity. The effects of added noise and waveform distortions are depicted in Fig. 10.11, where data waveforms were recorded using an analog oscilloscope.

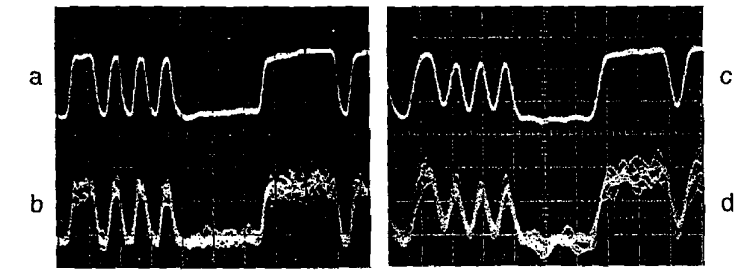

Fig. 10.11 Waveforms showing noise and intersymbol interference (ISI) effects. Waveform with (a) low noise and low distortion, (b) large noise and low distortion, (c) low noise and large distortion, and (d) large noise and large distortion.

The most accurate method of measuring margin in long-haul lightwave systems is the decision circuit method of measuring the Q factor (Bergano, Kerfoot, and Davidson 1993). The Q factor (adapted from Personick's work in 1973 on calculating the performance of receivers in lightwave links) is the argument to the normal error function for the purpose of calculating the BER. This is shown schematically in Figure 10.12. The Q factor is estimated using the regenerator's decision circuit to probe the rails of the data eye, and it includes the ISI present in the regenerator's linear channel as well as that generated in the system from dispersion and fiber nonlinearity. Figure 10.13 shows a Q-factor measurement of 7.2:1 (linear ratio), or 17.2 dB, for a 9000-km transmission experiment using 33-km amplifier spacing. The Q factor is estimated by measuring the BER at different threshold settings in the decision circuit; then the data are fitted with an ideal curve, assuming Gaussian noise statistics:

$$BER(V) = \frac{1}{2}\left[erfc\left(\frac{|\mu_1 - V|}{\sigma_1}\right) + erfc\left(\frac{|V - \mu_0|}{\sigma_0}\right)\right], \qquad (10.6)$$

where $erfc(x) = (1/\sqrt{2\pi}) \int_x^\infty e^{-\alpha^2/2}\, d\alpha$. The curve fit gives the equivalent values for the means ($\mu_{1,0}$) and standard deviations ($\sigma_{1,0}$) of the voltages on the marks and spaces in the data eye, and the Q factor is formed as

$$Q \equiv \frac{|\mu_1 - \mu_0|}{\sigma_1 + \sigma_0}. \qquad (10.7)$$

The Q factor given in Eq. (10.7) is unitless quantity expressed as a linear

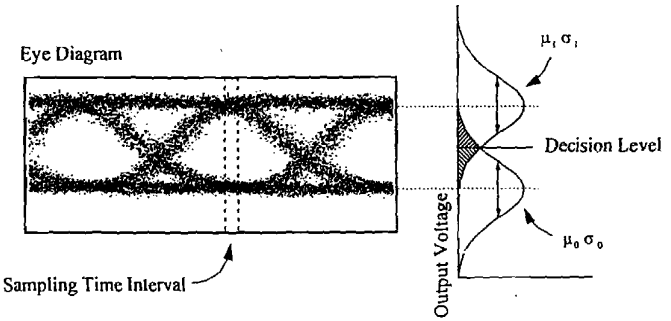

Fig. 10.12 Typical received eye diagram for an undersea lightwave system operating at 5 Gb/s. A voltage histogram is schematically shown to indicate the parameters that are included in the definition of the Q factor.

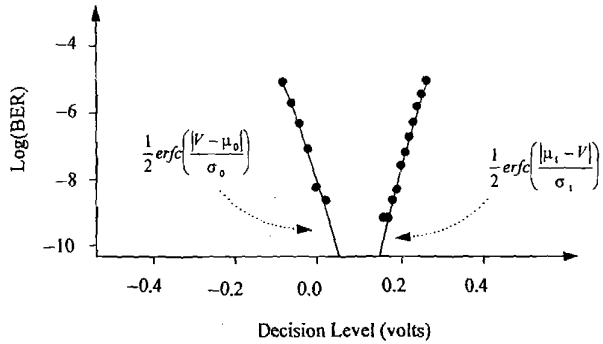

Fig. 10.13 Typical Q-factor measurement for 5-Gb/s, 9000-km operation. The data show the bit error rate (BER) versus the decision threshold at 9000 km. The *solid lines* show the fit of Eq. (10.6) to the data.

ratio, or it can be expressed in decibels as 20 log(Q). The factor of 20 (or 10 log[Q^2]) is used to maintain consistency with the linear noise accumulation model. For example, a 3-dB increase in the average launch power in all the spans results in a 3-dB increase in the Q factor (ignoring signal decay and fiber nonlinearity).

It is well known that the electrical noise at the decision circuit is not exactly Gaussian (Marcuse 1990); however, the Gaussian approximation can lead to close BER estimates (Humblet and Azizoglu 1991). Figure 10.14 shows the measured voltage histogram of a detected optical signal emerging from a long lightwave system operating at 5 Gb/s. For this measurement, 1-million voltage samples were recorded for a zero bit and a one bit in a 2^7-1 data pattern. The non-Gaussian probability density function is apparent when the actual density is compared with a best fit Gaussian. The measurement of the Q factor as described previously measures only a subset of the distributions located near "inside" rails of the received eye, or the voltages that are close to the decision circuit. Thus, the inside edges of the eye are fitted with an equivalent Gaussian function, and the underlying SNR is extrapolated from the fit.

Mazurczyk and Duff (1995) have identified the inability of the decision circuit Q-factor measurement to measure large margin using long data patterns. Pattern-dependent effects cause the Q-factor measurement to underestimate the actual Q factor for long pseudo-random data patterns with large margin. The cause of the effect is shown schematically in Fig.

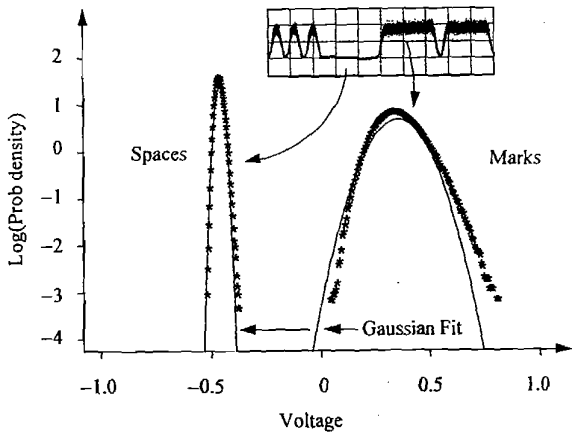

Fig. 10.14 Typical voltage histogram of a 5-Gb/s NRZ data signal for the ones and zeros rails.

10.15. In the figure, the upper part of the received eye diagram is expanded to show the ISI. In this diagram, the pattern dependence of the data causes different bits to have different mean voltages at the decision circuit's timing

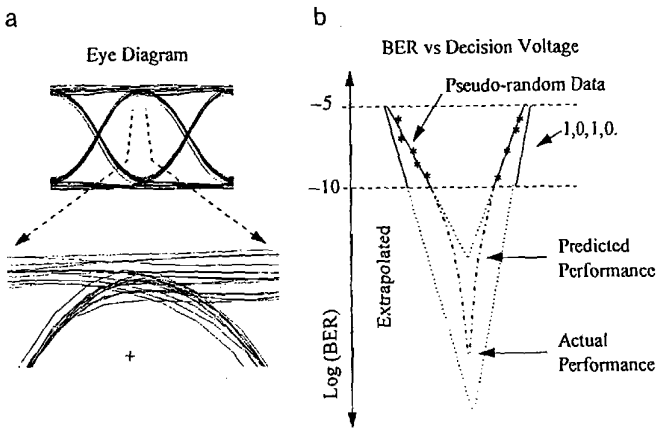

Fig. 10.15 (a) Expanded view of the upper rail of an eye diagram showing ISI. (b) The resulting BER versus decision level curve can have a slope change causing the Q-factor measurement to underestimate the actual value.

10.6 Polarization Effects

Several polarization effects in lightwave systems can combine to degrad the performance of long-haul lightwave systems. These effects can bot reduce the mean received SNR (Lichtman 1993b; Bruyere and Audoui 1994) and cause the SNR to fluctuate with time (Yamamoto *et al.* 1993) Standard telecommunications optical fibers do not maintain the state o polarization (SOP) of the transmitted signal. Random perturbations alon the fiber's length can couple the transmitted signal between the two polar ization modes and give rise to the time-varying SOP and polarization mod dispersion (PMD). The unstable polarization can interact with polarization dependent loss (PDL) in the EDFA's components and polarization hol burning (PHB) in the erbium fiber and give rise to the SNR fluctuations (See Chapter 6 in Volume IIIA for a more complete treatment of polariza tion effects in lightwave systems.)

SNR fluctuations in long-haul amplifier-based systems are unavoidabl because all practical systems use nonpolarization-maintaining transmissio fibers. SNR fluctuations must be accounted for in the design of the systen by reducing PDL and PMD where possible, and by building in additiona margin at the beginning of life of the system. Figure 10.16 shows a typica plot of the received Q factor versus time for a transatlantic-length transmis sion at 5 Gb/s. Peak-to-peak fluctuations of 1.5 dB are observed withou polarization scrambling at the transmitter (Taylor and Penticost 1994).

PHB can cause the ASE noise to accumulate in the polarization orthogo nal to the signal faster than along the parallel axis (Fig. 10.17). Nois accumulates faster than would be predicted by the simple noise accumula tion theory, and, as a result, the signal decays at the expense of the noise PHB results from an anisotropic saturation created when a polarized satu rating signal is launched into the erbium-doped fiber. The PHB effect wa first observed by Taylor (1993) as an excess noise accumulation in a chai of saturated EDFAs, and it was later isolated in a single amplifier an identified by Mazurczyk and Zyskind (1993). The gain difference cause by PHB is small in a single amplifier, with a typical value of about 0.07 dI for an amplifier with 3 dB of gain compression. Although PHB is a ver small effect in a single EDFA, its effect on the overall performance of a optical amplifier transmission line can be several decibels in the receive Q factor. This illuminates the basic difference between optical amplific and regenerative transmission systems: subtle effects in the amplifiers and or fibers can *accumulate* to cause significant impairments of the system's per formance.

point. The resulting BER versus decision voltage curve does not follow a simple Gaussian characteristic; rather, it follows the rules of total probability given each bit's probability density function. For large margins, the resulting curve can exhibit a slope change at BERs less than what is practical to measure, and the extrapolated BER and Q factor are then underestimated. In practice, this is not a serious limitation to characterizing a working system, because typical values of beginning-of-life optical margins are less than 5 or 6 dB. A practical engineering fix to this problem is to measure the Q factor for a series of word lengths.

The decision circuit method of measuring the Q factor is the most accurate measurement of system margin because the measurement is based on the BER, which considers every bit in the data sequence. The BER is routinely and accurately measured to 1 part in 10^{10}. Alternatives to this technique include other electrical SNR measurements such as voltage histograms and optical SNR measurements using optical spectrum analyzers. A voltage histogram down the center of the eye can be measured with a digital sampling oscilloscope to estimate the Q factor. However, this technique fails to give a good correlation between the measurement of the Q factor and the BER, because the variation seen around each rail represents a mix of pattern effects and noise. Such effects in turn artifically broaden the estimates of $\sigma_{1,0}$, thus giving erroneous results. In addition, this method operates on a limited set of bits (i.e., the data arrive at 5 Gb/s, while the oscilloscope's analog-to-digital converter samples at 10–100 kHz). Alternatively, the voltage histograms can be made at a specific point in the pattern as opposed to the data eye. This eliminates the pattern effects from the measurements of $\sigma_{1,0}$ but yields a potentially inaccurate measure of $\mu_{1,0}$. Also, this approach has the drawback of recording even fewer bits than the measurement in the eye, and it is not practical in a real transmission system, where the data bits are random.

It is often useful to know the ideal Q factor as a starting place for systems calculations. Humblet and Azizoglu (1991) described the ideal Q factor, considering only accumulated noise impairments in terms of the optical SNR_o (Eq. [10.3]) as

$$Q(dB) = 20 \log \left[\frac{2SNR_o\sqrt{B_o/B_e}}{1 + \sqrt{1 + 4SNR_o}} \right] \tag{10.8}$$

where B_o and B_e are the optical and electrical bandwidths in the receiver.

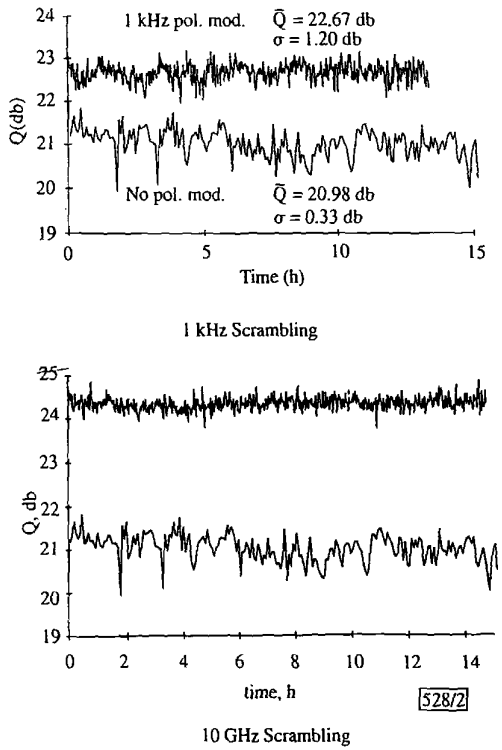

Fig. 10.16 Q-factor fluctuations using different polarization scrambling techniques. [*Top,* Adapted with permission from Taylor, M. G. 1994. Improvement in Q with low frequency polarization modulation on transoceanic EDFA link. *IEEE Photon. Tech. Lett.* 6(7):860, © 1994 IEEE; *bottom,* adapted with permission from Taylor, M. G., and S. J. Penticost, 1994. Improvement in performance of long haul EDFA link using high frequency polarization modulation. *Electron. Lett.* 30(10):805.]

Fortunately, the deleterious effects of PHB can be avoided by polarization modulation (or scrambling) of the signal at a rate faster than that to which the EDFA can respond. When the signal's polarization is scrambled faster than the amplifier can respond, there is no preferred polarization axis for the gain to be depleted, and the transmission performance returns to the expected value. The characteristic time constant associated with PHB is similar to the time constants that govern the large signal response of the EDFA, or about 130–200 μs. To reduce the negative effects of PHB on transmission systems, the SOP of the transmitted optical data signal should be scrambled at a rate that is high compared with the amplifier's response

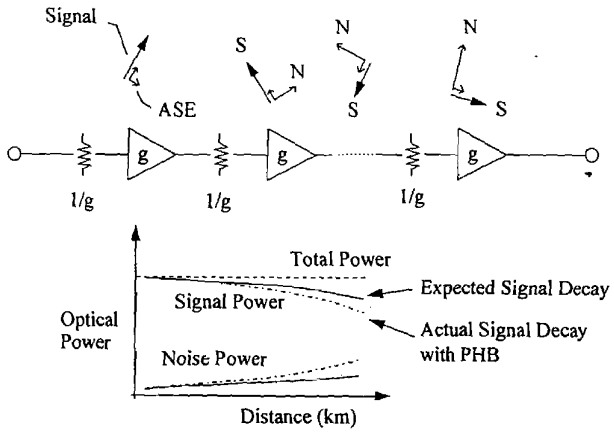

Fig. 10.17 Polarization hole burning (PHB) causes the noise in the orthogonal polarization to have an excess gain of ΔG per amplifier stage.

time. Therefore, polarization scrambling should interchange the optical signal between orthogonal polarizations at a frequency higher than (1/130 μs, or about 8 kHz. Thus, the frequency of polarization scrambling (on a great circle route around the Poincaré sphere; Kliger, Lewis, and Randall 1990) should be greater than 4 kHz to reduce the negative effects of PHB.

Although scrambling in the kilohertz range improves the PHB, it can also cause other effects that can negate any potential improvement. These include amplitude modulation (AM) of the data signal resulting from polarization modulation to AM conversion through the PDL elements in the system, and jitter caused from the interaction of the polarization scrambling and PMD (Bergano 1995b). Considering these phenomena, it is more desirable to scramble at rates equal to or faster than the data's bit rate so that the AM modulation occurs outside the receiver's bandwidth.

The first report of polarization scrambling to improve the performance of long EDFA transmission systems used a two-wavelength transmitter (Bergano, Davidson, and Li 1993). Since that time, other reports have confirmed the results using high-speed lithium niobate scramblers (Taylor and Penticost 1994; Fukada, Imai, and Mamoru 1994) and low-speed scramblers (Bergano *et al.* 1994). The optimal choice of the scrambling frequency is the clock frequency that defines the bit rate of the transmitter (Bergano *et al.* 1995). This technique is particularly important for the efficient use of optical bandwidth in WDM systems. Bit-synchronous polarization scrambling is the optimal trade-off between the two regimes of low-speed and high-speed scrambling. Scrambling the polarization at speeds lower than the bit rate reduces the effects of PHB but introduces unwanted AM through PDL in the optical elements of the system (Lichtman 1995). Scrambling at frequencies higher than the bit rate reduces the PDL problem (Taylor and Penticost 1994) but causes an increase in the transmitted bandwidth, which can limit the number of channels packed into a fixed optical bandwidth. In addition, synchronous polarization scrambling with superimposed phase modulation (PM) can dramatically increase the eye opening of the received data pattern. The increase in eye opening results from the conversion of PM into bit-synchronous AM through chromatic dispersion and nonlinear effects in the fiber.

10.7 Transmission Experiments

Most long-haul transmission experiments using optical amplifiers fall into one of three categories: circulating loops, test beds, and special measurements performed on installed systems. Circulating loop experiments were first performed in 1991 to demonstrate the feasibility of optical amplifier transmission systems. Then, in 1992 to 1993, long amplifier chains were constructed for laboratory use as a test bed for establishing design parameters and feasibility of monitoring systems concepts. Finally, special measurements were performed on the first installed amplifier systems in 1994 to 1995 to determine the feasibility of upgrading the system after its installation. This upgrade potential is unique to amplified systems because there are no bit-rate-limiting elements in the undersea amplified line.

Optical loop experiments were performed as early as 1977 to study pulse propagation in multimode fiber (Tanifuji and Ikeda 1977), jitter accumulation in digital fiber systems (Trischitta, Sannuti, and Chamzas 1988), optical soliton pulse propagation (Mollenauer and Smith 1988), and pulse propagation in single-mode fiber (Malyon *et al.* 1991). Loop transmission experiments became useful for optical amplifier feasibility demonstrations after techniques were developed to measure the BER of long pseudo-random data patterns (Bergano *et al.* 1991a, 1991b). A loop experiment attempts to simulate the transmission performance of a long system by reusing or recirculating an optical data signal through a modest-length amplifier chain ranging from tens to hundreds of kilometers. In the loop experiment (Fig. 10.18), optical switching is added to allow data to flow into the loop (the *load* state) or to allow data to circulate (the *loop* state). The data circulates

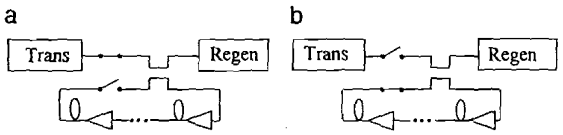

Fig. 10.18 Simplified block diagram of a loop transmission experiment, showing (a) the load state and (b) the loop state.

for a specified time, after which the state of the experiment toggles, and the load–loop cycle is repeated.

Figure 10.19 shows the BER versus transmission distance for a single-channel loop transmission experiment using the 264-km amplifier chain. For the 5 Gb/s transmission, a 10^{-9} BER was achieved at a transmission distance of 20,000 km, or 76 circulations through the amplifier chain. At this distance, the error counting duty cycle was 136:1; thus, an error-free interval of 68 s (real time) was required to demonstrate a 10^{-9} BER with 90% confidence. At 10 Gb/s, the 10^{-9} BER intercept distance was 10,400 km.

Circulating loop techniques can also be used to study WDM transmission. Figure 10.20 shows the block diagram of a 100-Gb/s transmission experiment where 20 5-Gb/s NRZ data channels were transmitted over 6300 km in 11.4 nm of optical bandwidth using a gain-flattened EDFA chain (Bergano *et al.* 1995). The transmission of many WDM channels over transoceanic distances can be limited by the finite bandwidth of the EDFA repeaters

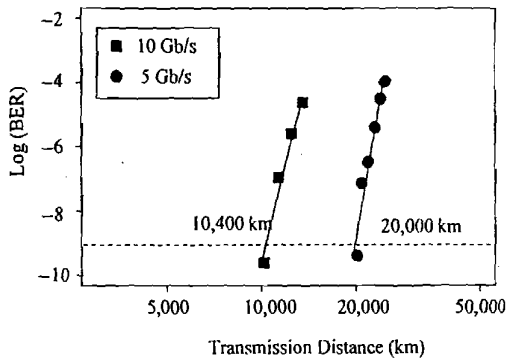

Fig. 10.19 BER versus transmission distance for the 264-km amplifier chain, at 5 and 10 Gb/s.

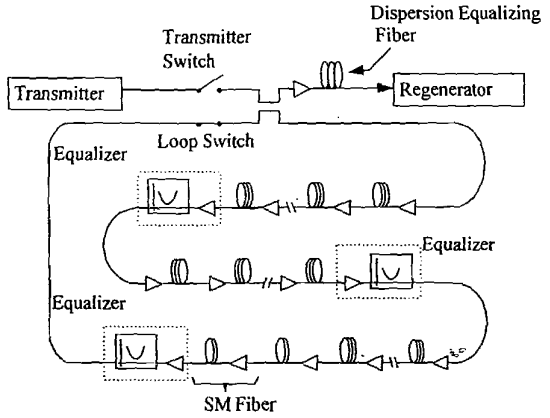

Fig. 10.20 Block diagram of the circulating loop used for a 100-Gb/s WDM transmission experiment.

and the nonlinear interactions between channels. In this experiment, the usable EDFA bandwidth was increased by a factor of 3 using long-period fiber grating filters (Vengsarkar, Lemaire, Jacobvitz, *et al.* 1995; Vengsarkar, Lemaire, Judkins, *et al.* 1995) as gain equalizers. The nonlinear interactions between channels were suppressed by using a transmission fiber with −2 ps/km-nm of dispersion (Bergano *et al.* 1995). Figure 10.21 shows the optical spectrum of the 20 WDM channels before and after propagation through 6300 km (i.e., five passes through the 1260-km amplifier chain).

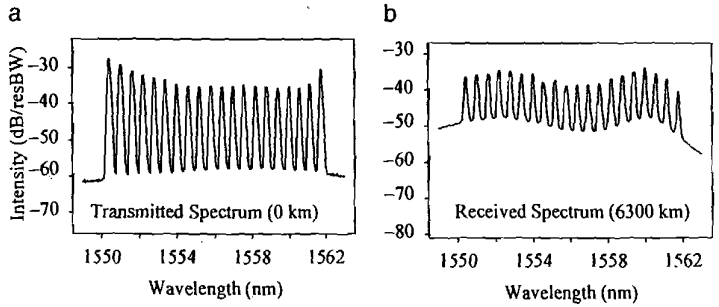

Fig. 10.21 Optical spectrum of 20 5-Gb/s data channels (a) before and (b) after transmission through 6300 km of fiber.

All 20 channels had a time-averaged BER better than 6×10^{-10}. The average Q factors ranged from 15.9 to 17.7 dB.

The performance of the 100-Gb/s WDM experiment was eventually extended to 9300 km using a low noise 980-nm pumped amplifier chain and a variety of the techniques described in this chapter. The transmission format used was NRZ with a combination of synchronous polarization modulation and amplitude modulation (Bergano *et al.* 1996). The gain equalized amplifier chain used 45-km amplifier spacing with a dispersion map similar to that shown in Fig. 10.10. The 980-nm EDFAs had an average noise figure of 4 dB and an output power of +8 dBm. Figure 10.22 shows measured Q-factors and corresponding bit error ratios for 20 5-Gb/s channels after 9300 km. At least 10 individual measurements were performed per channel over a time period long enough to have different polarization states. This procedure ensured an accurate measure of the average BER, considering the fluctuations of the received SNR from polarization effects. The *left-hand arrow* indicates the average Q-factor, and the *right-hand arrow* indicates the average BER over the entire measurement period. All 20 channels had a time-averaged BER lower than 10^{-11}, and the average Q-factor for all 20 channels was 17.4 dB.

Since the time of the initial feasibility studies using circulating loop experiments, several long test-bed experiments have been reported, where

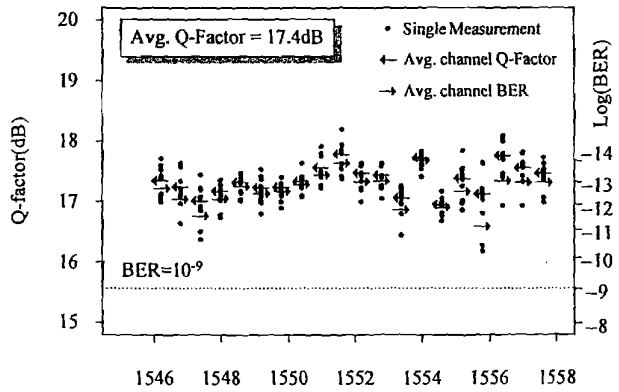

Fig. 10.22 The measured Q factor and corresponding BERs versus channel wavelength for the 20 5-Gb/s WDM NRZ channels at 9300 km. The average Q factors are indicated by the *left-hand arrows*, and the average BER are indicated by the *right-hand arrows*. The Q factor averaged over all 20 channels was 17.4 dB.

hundreds of amplifiers were concatenated to form amplifier chains up to 10,000 km long (Bergano *et al.* 1992; Imai *et al.* 1992). These experiments provided invaluable information on many of the design parameters in a long-haul system, including many of the entries in the impairment budget. The test-bed experiments provided the most accurate representation of the actual system performance; however, given the amount of equipment involved, test-bed experiments tend to be expensive. By contrast, transmission experiments performed using loop techniques require far fewer components, cost much less, and provide the flexibility of making measurements that are impractical in test-bed experiments. For example, the side-by-side comparison of two transmission fiber types or amplifier designs is more easily and economically made in a loop measurement than in a test bed, given the amount of equipment involved.

AT&T installed its first optical amplifier undersea systems in 1994 in the Caribbean. Two cables, each about 2100 km long, were installed as part of the Americas and Columbus systems. The Americas-1 North cable joined Vero Beach, Florida, to Magens Bay in St. Thomas, and the Columbus-IIB cable joined West Palm Beach, Florida, to Magens Bay, St. Thomas. The Columbus-IIB segment contains two fiber pairs and 26 repeaters with an average repeater spacing of 80 km. Each pair operates with a single 2.5-Gb/s NRZ optical channel at 1558.5 nm. The amplifiers have an output power of about +5 dBm at 18 dB of gain and 5.7 dB of noise figure. Measurements performed with a higher bit-rate terminal and using WDM techniques demonstrated that this system could operate at up to 15 Gb/s, or six times its designed capacity (Jensen *et al.* 1995).

Similar measurements were also performed on a 4200-km installed cable section of the Trans-Pacific Cable (TPC-5) system (Feggeler *et al.* 1996). Segment G of TPC-5 is installed between San Luis Obispo, California, and Keawaula, Hawaii. Tests performed at transmission rates up to 10 Gb/s and at distances up to 16,800 km (by looping the received signal back at each end) demonstrated that the cable segment is fully capable of operating at twice the design line rate of 5 Gb/s.

10.8 Transmission Systems

Thus far, we reviewed several aspects of optical amplifier transmission technology used in undersea cable systems. This section attempts to put the pieces together by reviewing the design of a typical transoceanic 5-Gb/s

NRZ transmission system. To this end, we use the TAT-12/13 cables as a model. The TAT-12/13 cables form a ring network in the north Atlantic with two transatlantic cables of 5900 km and 6300 km, and two interconnection cables, each a few hundred kilometers in length (Trischitta *et al.* 1996) (Fig. 10.23). The ring architecture allows for mutual restoration capability *within the network* with the use of network protection elements at each of the four landing sights. In the unlikely event of a cable failure, the customer's traffic is automatically rerouted in the opposite direction around the ring to bypass a fault in any of the undersea segments. The name TAT-12/13 signifies that they are 12th and 13th transatlantic telephone systems installed in the Atlantic by AT&T and its partners. The TAT-12 cable is one of the first major applications of EDFA technology in the undersea market. The TAT-12/13 cable system is owned and operated by a consortium of 44 partners, and was designed and manufactured by AT&T Submarine Systems, Alcatel Submarine Networks, and Toshiba. The network was placed into service in September 1996.

Undersea cable systems are designed with a 25-year life expectancy. The goal of the system design is to have an adequate beginning-of-life margin to allow for Q-factor fluctuations, component aging, and system repairs. Key design parameters are the repeater spacing, the launch power, and the dispersion management of the repeatered line. The trade-offs in the selection of the repeater spacing are cost and performance. Increasing the repeater spacing reduces cost and improves reliability because fewer repeaters

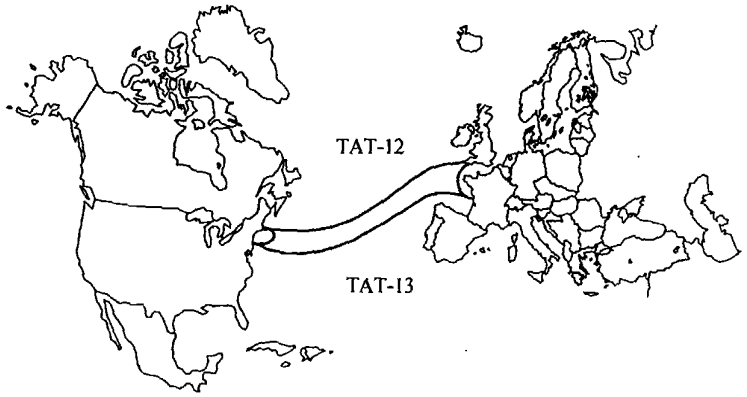

Fig. 10.23 TAT-12/13 cable system.

are needed; however, fewer repeaters mean longer repeater spacing, which translates into more accumulated noise. For a particular system, the repeater spacing is chosen as the largest length possible, satisfying the end-of-life requirement, given in the impairment budget. Performance is measured against the Q factor of 16.1 dB or the value relating to a BER of 1×10^{-10}.

The impairment budget is a design tool used to aid in the selection of span length by accounting for all the expected impairments over the system's lifetime. An impairment budget is given in Table 10.2. The starting point is the ideal Q factor, which is calculated considering only optical noise using Eqs. (10.3) and (10.8). In our example, this value is 30.5 dB, assuming a 6300-km system with 45-km repeater spacing, +3-dBm output power, a 5.4-dB noise figure, and 0.2-dB/km fiber attenuation. From this starting point the values of all expected degradations are subtracted. For example, the 8.7-dB value in line 2 includes effects arising from the fiber's nonlinear index, added noise from optical reflections, ISI, and Q-factor fluctuations caused by polarization effects. This value is obtained using data from laboratory experiments and computer modeling. The values in the table are recalculated for different span lengths until the 1-dB end-of-life figure is

Table 10.2 **Performance Budget for a 5-Gb/s Transmission System**[a]

Line	*Parameter*	*Value or Penalty (dB)*
1	Ideal Q factor (dB)	30.5
2	Interactive and fluctuation impairments	−8.7
3	Worst case nonimpaired Q factor (1 + 2)	21.8
4	Beginning-of-life (BOL) impairments: Line design margin, transmitter–receiver design margin, loop-back path impairments, etc.	−3.5
5	Unallocated margin	−0.5
6	Minimum BOL performance (3 + 4 + 5)	17.8
7	Aging and repairs	−0.7
8	Minimum end-of-life (EOL) performance (6 + 7)	17.1
9	Required Q factor for bit error rate (BER) $<1 \times 10^{-10}$	16.1
10	EOL margin (8 − 9)	1.0

[a] Adapted from Schesser *et al.* 1995.

reached. If forward error-correction coding is used in the terminals, the value on line 9 could be lowered to 11.4 dB, corresponding to an uncorrected BER of 10^{-4}.

Long undersea cable systems include a monitoring capability to ascertain the performance of the cable and repeaters and to locate faults in the event of a cable break or component failure (Chapters 2 and 3 in Volume IIIB). In the AT&T system design, high-loss loop-back paths joining the amplifiers in a pair allow a small amount of signal (−45 dB) to leak back in the opposite direction with a unique round-trip delay (Jensen *et al.* 1994). The amplitude of the out-going 5-Gb/s data signal is modulated with a low-frequency pseudo-random bit pattern located on a 2-MHz subcarrier. When digital signal processing techniques are used at the terminal, the small amount of in-coming signal is correlated with the transmitted signal, and the gain of each loop-back path is measured. When the system is in service, the depth of modulation is only a few percent. For out-of-service operation, the depth of modulation is increased to 100% to speed up the measurement time.

Each transatlantic cable has four chains of amplifiers, grouped as two bidirectional pairs. Each of the four fibers carries a single 5-Gb/s NRZ data signal. The amplifiers are spaced at 45-km intervals along the cable (Table 10.3) and are located in repeater pressure vessels that can withstand up to 800 atmospheres of pressure found at the ocean bottom. Repeaters are powered by passing a 0.9-A DC current through a power conductor within the cable. The amplifiers have a nominal gain of 9.5 dB and a noise figure of 5 dB, at an output power of about +3 dBm, and at 5 dB of gain compression. The transmission fiber is single-mode dispersion-shifted fiber, selected to have a dispersion value of about −0.3 ps/km-nm on average.

Table 10.3 **Repeater Spacing for Existing Optical Amplifier Undersea Transmission Systems**

System	*Bit Rate (Gb/s)*	*System Length (km)*	*Repeater Spacing (km)*
TPC-5 segment J	5.0	8620	33
TAT-12/13	5.0	5900/6300	45
TPC-5 segment G	5.0	4200	68
TPC-5 segment T1	5.0	1300	82

This small amount of negative dispersion reduces the nonlinear mixing between the signal and the optical noise. The accumulated negative dispersion is compensated for every 500 km using normal single-mode fiber with $\lambda_0 = 1310$ nm.

Each fiber pair carries a single NRZ channel operating at a bit rate of 4.97664 Gb/s, comprised of two STM-16 (2.48832 Gb/s) bit interleaved. Thus, each cable with its two fiber pairs carries a total of 4 STM-16 channels. Since the TAT-12/13 network is designed to have mutual restoration capability within the network, each cable is configured with one pair designated for normal traffic and one pair for restoration. Each STM-16 channel consists of 30,240 64-kB/s digital circuits (calculated by multiplying 30 64-kB/s circuits per E1, 63 E1s in an STM-1, and 16 STM-1s in an STM-16). The network has 4 STM-16 primary channels for normal traffic, which is 120,960 64-kB/s circuits. These circuits configured to carry voice traffic only would support about 600,000 simultaneous conversations (using a compression ratio of 5:1), with an additional 600,000 voice circuits available for standby traffic on the protection lines.

10.9 Summary

The first generation of optical amplifier undersea lightwave systems has now been deployed in both the Atlantic and the Pacific oceans. These first systems operate at 5 Gb/s, which is about 300,000 equivalent voice circuits per fiber pair. Technical innovations such as WDM transmission will allow the transmission capacity of undersea cable systems to increase 20-fold in the next few years. As the demand for newer advanced digital services expands in the national markets, so too will the demand grow for these services in the international market. Lightwave transmission systems based on optical amplifier repeaters will provide the international conduits for these new services.

The reader who is interested in a more detailed understanding of optical amplifier undersea cable systems is directed to review an issue of *IEEE Communications Magazine* that includes information on Global Undersea Communication Networks (Trischitta and Marr 1996), a special issue of the *AT&T Technical Journal* (AT&T 1995), and Thiennot, Pirtio, and Thomine (1993). For a good review of amplifier systems in general, see Li (1993).

References

Agrawal, G. P. 1989a. Group-velocity dispersion. In *Nonlinear fiber optics,* Chapter 3. Boston: Academic Press, 51–73.

Agrawal, G. P. 1989b. *Nonlinear fiber optics.* Boston: Academic Press.

AT&T. 1995. Undersea communications systems. *AT&T Tech. J.* 74(1).

Bell Telephone Laboratories. 1982. *Transmission systems for communications.* 5th ed. Holmdel, NJ: Bell Telephone Laboratories, Inc., 741.

Bergano, N. S., J. Aspell, C. R. Davidson, P. R. Trischitta, B. M. Nyman, and F. W. Kerfoot. 1991a. Bit error rate measurements of a 14,000 km 5 Gb/s fiber-amplifier transmission system using a circulating loop. *Electron. Lett.* 27(21):1889.

Bergano, N. S., J. Aspell, C. R. Davidson, P. R. Trischitta, B. M. Nyman, and F. W. Kerfoot. 1991b. A 9000 km 5 Gb/s and 21,000 km 2.4 Gb/s feasibility demonstration of transoceanic EDFA systems using a circulating loop. In *OFC '91, San Diego, CA.* Postdeadline paper PD13, PD13-1.

Bergano, N. S., and C. R. Davidson. 1995. Polarization scrambling induced timing jitter in optical amplifier systems. In *OFC '95, San Diego, CA.* Paper WG3, 122.

Bergano, N. S., C. R. Davidson, and F. Heismann. 1996. Bit-synchronous polarization and phase modulation scheme for improving the transmission performance of optical amplifier transmission system. *Electron. Lett.* 32(1).

Bergano, N. S., C. R. Davidson, G. M. Homsey, D. J. Kalmus, P. R. Trischitta, J. Aspell, D. A. Gray, R. L. Maybach, S. Yamamoto, H. Taga, N. Edagawa, Y. Yoshida, Y. Horiuchi, T. Kawazawa, Y. Namihira, and S. Akiba. 1992. 9000 km, 5 Gb/s NRZ transmission experiment using 274 erbium-doped fiber-amplifiers. In *Optical amplifiers and their applications topical meeting, Santa Fe, NM.* Postdeadline paper PD11.

Bergano, N. S., C. R. Davidson, and T. Li. 1993. A two-wavelength depolarized transmitter for improved transmission performance in long-haul EDFA systems. In *LEOS '93 annual meeting, San Jose, CA, November 1993.* Postdeadline paper PD2.2, 23.

Bergano, N. S., C. R. Davidson, *et al.* 1995. 40 Gb/s WDM transmission of eight 5 Gb/s data channels over transoceanic distances using the conventional NRZ modulation format. In *OFC '95, San Diego, CA.* Paper PD19.

Bergano, N. S., C. R. Davidson, A. M. Vengsarkar, B. M. Nyman, S. G. Evangelides, J. M. Darcie, M. Ma, J. D. Evankow, P. C. Corbett, M. A. Mills, G. A. Ferguson, J. R. Pedrazzani, J. A. Nagel, J. L. Zyskind, J. W. Sulhoff, and A. J. Lucero. 1995. 100 Gb/s WDM transmission of twenty 5 Gb/s NRZ data channels over transoceanic distances using a gain flattened amplifier chain. In *European Conference on Optical Communication (ECOC '95), Brussels, Belgium,* Paper Th.A. 3.1, 967.

Bergano, N. S., F. W. Kerfoot, and C. R. Davidson. 1993. Margin measurements in optical amplifier systems. *IEEE Photon. Tech. Lett.* 5(3):304.

Bergano, N. S., V. J. Mazurczyk, and C. R. Davidson. 1994. Polarization scrambling improves SNR performance in a chain of EDFAs. In *OFC '94, San Jose, CA.*

Bruyere, F., and O. Audouin. 1994. Penalties in long-haul optical amplifier systems due to polarization dependent loss and gain. *IEEE Photon. Tech. Lett.* 6(5):654.

Ehrbar, R. D. 1986. Undersea cables for telephony. In *Undersea lightwave communications,* chapter 1. New York: IEEE Press.

Feggeler, J. C., D. G. Duff, N. S. Bergano, C. Chen, Y. Chen, C. R. Davidson, D. G. Ehrenberg, S. J. Evangelides, G. A. Ferguson, F. L. Heismann, G. M. Homsey, H. D. Kidorf, T. M. Kissell, A. E. Meixner, R. Menges, J. L. Miller, O. Mizuhara, T. V. Nguyen, B. M. Nyman, Y. K. Park, W. W. Patterson, and G. F. Valvo. 1996. 10 Gb/s WDM transmission measurements on an installed optical amplifier undersea cable system. In *OFC '96, San Jose, CA.* Paper TUN3, 72.

Fukada, Y., T. Imai, and A. Mamoru. 1994. BER fluctuation suppression in optical in-line amplifier systems using polarization scrambling technique. *Electron. Lett.* 30(5):432.

Giles, C. R., and E. Desurvire. 1991. Propagation of signal and noise in concatenated erbium-doped fiber amplifiers. *J. Lightwave Tech.* 9(2):147.

Giles, C. R., E. Desurvire, and J. Simpson. 1989. Transient gain and cross talk in erbium-doped fiber amplifier. *Opt. Lett.* 14(16):880.

Gordon, J. P., and L. F. Mollenauer. 1990. Phase noise in photonic communications systems using linear amplifiers. *Opt. Lett.* 15(23):1351.

Gordon, J. P., and L. F. Mollenauer. 1991. Effects on fiber nonlinearities and amplifier spacing on ultra-long distance transmission. *J. Lightwave Commun.* 9(2):170.

Humblet, P. A., and M. Azizoglu. 1991. On the bit error rate of lightwave systems with optical amplifiers. *J. Lightwave Tech.* 9:1576.

Imai, T., M. Murakami, Y. Fukada, M. Aiki, and T. Ito. 1992. Over 10,000 km straight line transmission system experiment at 2.5 Gb/s using in-line optical amplifiers. In *Optical amplifiers and their applications topical meeting, Santa Fe, NM.* Postdeadline paper PD12, PD-12.

Jensen, R. A., C. R. Davidson, D. L. Wilson, and J. K. Lyons. 1994. Novel technique for monitoring long-haul undersea optical-amplifier systems. In *Optical Fiber Communications Conference, San Jose, CA.* Paper ThR3.

Jensen, R. A., D. G. Duff, J. J. Risko, and C. R. Davidson. 1995. Possibility for upgrade of the first installed optical amplifier system. In *Topical meeting on optical amplifiers and their applications, Davos, Switzerland.* Paper ThB2, 9.

Kaiser, P., and D. B. Keck. 1988. Fiber types and their status. In *Optical fiber telecommunications II,* ed. S. E. Miller and I. P. Kaminow, 29–51. Boston: Academic Press.

Kawai, S., K. Iwatsuki, K. Suzuki, S. Nishi, M. Saruwatari, K. Sato, and K. Wakita. 1994. 10 Gbit/s optical soliton transmission over 7200 km by using a monolithically integrated MQW-DFB-LD/MQW-EA modulator light source. *Electron. Lett.* 30(3):251.

Kliger, D. S., J. W. Lewis, and C. E. Randall. 1990. *Polarized light in optics and spectroscopy*. New York: Academic Press.

Kodama, Y., and A. Hasegawa. 1992. Generation of asymptotically stable optical solitons and suppression of the Gordon-Haus effect. *Opt. Lett.* 17:31.

Li, T. 1993. The impact of optical amplifiers on long-distance lightwave telecommunications. *Proc. IEEE* 18(11):1568.

Lichtman, E. 1993a. Optimal amplifier spacing in ultra-long lightwave systems. *Electron. Lett.* 29:2058.

Lichtman, E. 1993b. Performance degradation due to polarization dependent gain and loss in lightwave systems with optical amplifiers. *Electron. Lett.* 29(22):1971.

Lichtman, E. 1995. Limitations imposed by polarization-dependent gain and loss on all-optical ultra-long communication systems. *J. Lightwave Tech.* 13(5).

Malyon, D., T. Widdowson, E. G. Bryant, S. F. Carter, J. V. Wright, and W. A. Stallard. 1991. Demonstration of optical pulse propagation over 10,000 km of fiber using recirculating loop. *Electron. Lett.* 27(2):120.

Marcuse, D. 1990. Derivation of analytical expressions for the bit-error probability in lightwave systems with optical amplifiers. *J. Lightwave Tech.* 8:1816.

Marcuse, D., A. R. Chraplyvy, and R. W. Tkach. 1991. Effects of fiber nonlinearity on long-distance transmission. *J. Lightwave Tech.* 9(1):121.

Mazurczyk, V. J., and D. G. Duff. 1995. Effect of intersymbol interference on signal-to-noise measurements. In *OFC '95, San Diego, CA.* Paper WQ1, 188.

Mazurczyk, V. J., and J. L. Zyskind. 1993. Polarization hole burning in erbium doped fiber amplifiers. *CLEO '93, Baltimore.* Postdeadline paper CPD26.

Mecozzi, A., J. D. Moores, H. A. Haus, and Y. Lai. 1991. Soliton transmission control. *Opt. Lett.* 16:1841.

Mollenauer, L. F., J. P. Gordon, and S. G. Evangelides. 1992. The sliding-frequency guiding filter: An improved form of soliton jitter control. *Opt. Lett.* 17:1575–1577.

Mollenauer, L. F., M. J. Neubelt, M. Haner, E. Lichtman, S. G. Evangelides, and B. M. Nyman. 1991. Demonstration of error-free soliton transmission at 2.5 Gb/s over more than 14,000 km. *Electron. Lett.* 27(22):2055.

Mollenauer, L. F., and K. Smith. 1988. Demonstration of soliton transmission over more than 4000 km in fiber with loss periodically compensated by Raman gain. *Opt. Lett.* 13(8):675.

Personick, S. D. 1973. Receiver design for digital fiber optic communications systems. *Bell Syst. Tech. J.* 52(6).

Runge, P. K., and P. R. Trischitta. 1986. The SL undersea lightwave system. In *Undersea lightwave communications,* New York: IEEE Press.

Schesser, J., S. M. Abbott, R. L. Easton, and M. S. Stix. 1995. Design requirements for the current generation of undersea cable systems. *AT&T Tech. J.* 74(1):16.

Taga, H., M. Suzuki, Y. Yoshida, H. Tanaka, S. Yamamoto, and H. Wakabayashi. 1991. 2.5 Gb/s optical transmission using electroabsorption modulator over 11,000 km EDFA systems. In *Conference on Lasers and Electro-Optics.* Paper CPDP38. Technical Digest. Washington, DC: Optical Society of America.

Tanifuji, T., and M. Ikeda. 1977. Pulse circulation measurement of transmission characteristics in long optical fibers. *Appl. Opt.* 16(8):2175.

Taylor, M. G. 1993. Observation of new polarization dependence effect in long haul optically amplified system. In *OFC '93, San Jose, CA.* Post deadline paper PD5.

Taylor, M. G. 1994. Improvement in Q with low frequency polarization modulation on transoceanic EDFA link. *IEEE Photon. Tech. Lett.* 6(7):860.

Taylor, M. G., and S. J. Penticost. 1994. Improvement in performance of long haul EDFA link using high frequency polarization modulation. *Electron. Lett.* 30(10):805.

Thiennot, J., F. Pirtio, and J. B. Thomine. 1993. Optical undersea cable systems trends. *Proc. IEEE* 81(11):1610.

Trishitta, P. R., M. Colas, M. Green, G. Wuzniak, and J. Arena. 1996. The TAT-12/13 cable network. *IEEE Communications Magazine.* 34(2):24.

Trischitta, P. R., and W. C. Marra. 1996. Global undersea communications networks. *IEEE Communications Magazine.* 34(2).

Trischitta, P. R., P. Sannuti, and C. Chamzas. 1988. A circulating loop experimental technique to simulate the jitter accumulation of a chain of fiber optic regenerators. *IEEE Trans. Commun.* COM-36:2.

Vengsarkar, A. M., P. J. Lemaire, G. Jacobovitz, J. J. Veselka, V. Bhatia, and J. B. Judkins. 1995. Long-period fiber gratings as gain-flattening and laser stabilizing devices. In *Proceedings of the IOOC '95,* vol. 5, 3–4. Hong Kong.

Vengsarkar, A. M., P. J. Lemaire, J. B. Judkins, J. E. Sipe, and T. Erdogan. 1995. Long-period fiber gratings as band-rejection filters. In *OFC '95, San Diego, CA.* Paper PD4.

Widdowson, T., and D. J. Malyon. 1991. Error ratio measurements over transoceanic distances using recirculating loop. *Electron. Lett.* 27(24):2201.

Yamamoto, S., N. Edagawa, H. Taga, Y. Yoshida, and H. Wakabayashi. 1993. Observation of BER degradation due to fading in long-distance optical amplifier system. *Electron. Lett.* 29(2):209.